Cross Correlating 21 cm Intensity Mapping fields with Kinematic Sunyaev-Zel'dovich Effect: Probing Missing Baryons at $z \sim 1-2$

Dongzi Li,[1,2] Ue-Li Pen,[3,4,5,1] Hong-Ming Zhu,[6,7] and Yu Yu[8]

[1]*Perimeter Institute for Theoretical Physics, 31 Caroline St. N., Waterloo, ON, N2L 2Y5, Canada*
[2]*University of Waterloo, 200 University Ave W, Waterloo, ON, N2L 3G1, Canada*
[3]*Canadian Institute for Theoretical Astrophysics, 60 St. George Street, Toronto, Ontario M5S 3H8, Canada*
[4]*Dunlap Institute for Astronomy and Astrophysics, 50 St. George Street, Toronto, Ontario M5S 3H4, Canada*
[5]*Canadian Institute for Advanced Research, CIFAR Program in Gravitation and Cosmology, Toronto, Ontario M5G 1Z8, Canada*
[6]*Key Laboratory for Computational Astrophysics, National Astronomical Observatories, Chinese Academy of Sciences, 20A Datun Road, Beijing 100012, China*
[7]*University of Chinese Academy of Sciences, Beijing 100049, China*
[8]*Key laboratory for research in galaxies and cosmology, Shanghai Astronomical Observatory, Chinese Academy of Sciences, 80 Nandan Road, Shanghai 200030, China*

(Dated: September 26, 2016)

The kinematic Sunyaev-Zel'dovich (kSZ) effect on cosmic microwave background (CMB), induced by radial momentum of hot electrons, is a powerful tracer to probe baryon distributions. However, the signal is weak and lack of redshift information, hence another survey with spectroscopic redshift is typically required. This largely limits the sky area and depth to harness kSZ. Here, we propose a new source for cross correlation— H I density field from 21 cm intensity mapping. 21 cm spectra provide accurate redshift and intensity mappings integrate weak diffuse spectra, and thus can survey large sky area with great depth in much shorter time with low costs.

One main concern of the method is that the complicate 21 cm foregrounds will contaminate radial large scale information, and reduce the correlation with kSZ. For redshift 1 and 2, we model the noise filtering in simulations, and find out that after velocity reconstructions, there is $\gtrsim 0.7$ correlation with kSZ signal for $\ell \gtrsim 800$, and it drops for smaller ℓ. To improve the correlation for smaller ℓ, we recover large scale modes from their tidal influence on small scale structures (Cosmic Tidal Reconstruction). Successfully recover $> 90\%$ information at $k \sim 0.01h/Mpc$, we obtain a correlation $r \sim 0.6-0.8$ for $\ell \sim 100-2000$. The overall S/N for $\ell \sim 300-4000$ assuming Planck noise scale can reach 45 at $z = 1$, and 59 at $z = 2$. Since the reconstructed field and foreground filtered field are superior in different modes, it is easy to combine them and improve S/N for $\ell \sim 1000$.

PACS numbers:

I. INTRODUCTION

For $z \lesssim 2$, large fractions of predicted baryon contents are missing in observations. The majority of them are believed to reside in warm-hot intergalactic mediums (WHIM) with typical temperature of 10^5 K to 10^7 K [1, 2]. High temperature and low density in the medium make us difficult to derive information from metal absroption lines, and uncertainties in ionization states and metalicity will also reduce the reliability. We are looking for signals that not only trace the majority of the baryons, but also easy to interprete.

Among the proposed candidates, the kinematic Sunyaev-Zel'dovich (kSZ) effect [3–5] is a promising one. kSZ effect results from Compton scattering of cosmic microwave background (CMB) off free electrons. The radial velocity of electrons will give photon a Doppler shift and hence leads to a secondary anisotropy in CMB temperature.

KSZ signal is ideal to tackle this problem for three reasons. First, it contributes from all the free electrons, indicating the distribution of 90% of the baryons in ionized states, leaving alone only less than 10% of baryons that reside in stars, remnants, atomic and molecular gases [6]. Second, the signal is mainly influenced by electron density and radial velocity, regardless the temperature, pressure and metalicity, so no extra assumptions are needed to estimate baryon abundance. Third, the peculiar velocity is dominantly related to large scale structures, therefore the signal is less biased towards local mass contraction.

Attractive as it is, two big drawbacks largely reduce the feasibility of harnessing kSZ signal. First, the signal is very weak and hence suffers seriously from contaminations from primary CMB, facility noises, thermal SZ effect, CMB lensing, etc. Second, it is an integrated effect along line of sight, therefore, kSZ itself does not contain redshift information.

A straight-forward mitigation of the two disadvantages is to cross-correlate kSZ signal with another tracer, which has both large scale structure and redshift information. Previous work has proposed optical spectroscopic survey as an ideal tool [7–9]. However, first, it lacks detectable spectral lines in redshift $1.4-2.5$, therefore unable to consistently measure until $z \sim 2$. Moreover we need large sky coverage to compensate for the weakness of kSZ signal, and the low efficiency of spectroscopic survey will make it unaccessible for near future. In this paper we discuss a new possibility for cross correlation—HI density field from 21 cm intensity mapping. HI 21 cm spectra have accurate redshift information, and are fully accessible for $z \lesssim 2$. Intensity mapping is a kind of survey that integrates all the signals in a pixel, rather than distinguishing individual galaxies. It can reach high S/N much faster, hence is very efficient for large sky surveys. There are already several ongoing experiments aim at large sky coverage and claim to be able to reach $z \gtrsim 2$ in very near future, such as CHIME [**?**], Tianlai [10], HIRAX [11] etc.

However, as feasibility is usually traded from data quality,

there are three main challenges for the upcoming H I surveys in terms of cross correlation with kSZ. First, the integration of different signals will cause complicated foregrounds, which would smear the large scale structure in radial direction[12, 13]. Second, the angular resolution is also supressed by the integration, droping information of small scale structure in transverse plane. Third, till now, the proposed experiments all work on interferometers, which drain the largest scale structure on transverse plane due to the finite length of the shortest baseline.

On the other hand, the most prominate kSZ signal that could be distinguished from noises contributes mainly from largest structure in radial direction with $l < 100$ and $l \sim 1000$. These modes are seriously damaged in intensity mapping due to the three challenges.

In this paper, we discuss the level of correlation we will get between kSZ and 21cm intensity mappings of different conditions. To lower the requirements on observational experiments, we use a method, cosmic tidal reconstruction [14, 15], to recover some of the large scale structure from its tidal force on small scales.

The paper is organized as follows: In section II, we demonstrate given a density field, how to correlate it with kSZ signal with velocity reconstruction, similar to [8]; we then estimate which modes dominates the produced signal; In section III, we present the result of cross correlation with foreground filtered field, different resolutions, and different shortest baselines and discuss the behavior; Then in section IV, we introduce the method of 3D tidal reconstruction, and present the correlation results after small k modes recovered, In section VI, we estimate statistical error and calculate S/N; and we conclude at section VII.

Notes: Throughout the paper, We use the $z = 1, 2$ output of six N-body simulations from the CUBEP^{3}M code [16], each evolving 1024^3 particles in a $(1.2\mathrm{Gpc}/h)^3$ box. Simulation parameters are as follows: Hubble parameter $h = 0.678$, baryon density $\Omega_b = 0.049$, dark matter density $\Omega_c = 0.259$, amplitude of primordial curvature power spectrum $A_s = 2.139 \times 10^{-9}$ at $k_0 = 0.05\ \mathrm{Mpc}^{-1}$ and scalar spectral index $n_s = 0.968$.

we use "$\wedge$" to denote recontructed fields as oppose to fields directly from simulations.

II. ALGORITHM: KSZ CROSS CORRELATION

In this section, we present a holographic method to cross correlate kSZ with a density field, following [8].

The CMB temperature fluctuations caused by kSZ effect is:

$$\Theta_{kSZ}(\hat{n}) \equiv \frac{\Delta T_{kSZ}}{T_{\mathrm{CMB}}} = -\frac{1}{c}\int d\eta g(\eta) \boldsymbol{p}_{\parallel}\ , \tag{1}$$

where $\eta(z)$ is the comoving distance at redshift z, $g(\eta) = e^{-\tau} d\tau/d\eta$ is the visibility function, τ is the optical depth to Thomson scattering, $\boldsymbol{p}_{\parallel} = (1+\delta)\boldsymbol{v}_{\parallel}$, with δ the electron overdensity, $\parallel$ indicates direction parallel to line of sight. We assume that $g(\eta)$ doesn't change significally in one redshift bin, and integrate $\boldsymbol{p}_{\parallel}$ along radial axis to get $\hat{\Theta}_{kSZ}$

Due to the cancellation of positive and negative velocity, its direct cross correlation between kSZ signal will vanish. To take advantage of the known redshift and better maintain the one to one multiplication between velocity field and density contrast, we generate a mock kSZ signal from calculation of linear peculiar velocity. In this way, we can at most maximize the correlation.

Assume we have a density contrast field $\delta = (\rho - \bar{\rho})/\bar{\rho}$, where $\bar{\rho}$ is the average density of a certain redshift slice.

Detailed steps are as follows.

(1) Estimate the velocity field:

In linear region, the continuity equation goes like: $\dot{\delta} + \nabla \cdot \boldsymbol{v} = 0$, where $\boldsymbol{v}$ is the peculiar velocity and δ is the matter overdensity.

Therefore, we obtain an estimator of velocity distribution from the density contract δ:

$$\hat{v}_z(\boldsymbol{k}) = iaHf\delta(\boldsymbol{k})\frac{k_z}{k^2} \tag{2}$$

where $f = d\mathrm{ln}D/d\mathrm{ln}a$, $D(a)$ is the linear growth function, a is the scale factor, H is the Hubble parameter.

$v_z \propto k_z/k^2$, indicating the most prominent signal comes from small k mode, which corresponds to large scale structure.

(2) Suppress the noise in velocity field with a Wiener filter. This is because the term k_z/k^2 in Eq.(2) will strongly amplify noises in small k modes.

$$\hat{v}_z^c(\boldsymbol{k}) = \frac{\hat{v}_z(\boldsymbol{k})}{b(k_\perp, k_\parallel)} W(k_\perp, k_\parallel)\ , \tag{3}$$

Bias $b = P_{\hat{v}_z, v_z}/P_{v_z}$, Wiener filter $W = P_{v_z}/(P_{\hat{v}_z}/b^2)$.

(3) Calculate 2D kSZ map follow Eq.(1).

(4) Calculate correlation coefficients.

We compare reconstructed kSZ signals $\hat{\Theta}_{kSZ}$ with kSZ signals Θ_{kSZ} directly from simulations. To quantify the tightness of correlation, we employ a quantity r:

$$r \equiv \frac{P_{recon,real}}{\sqrt{P_{recon}P_{real}}} \tag{4}$$

III. CONDITION: KSZ + 21CM INTENSITY MAPPING

In this section, we discuss the origin of kSZ signal on different structure scales, and compare it with scales resolvable in ongoing 21cm Intensity Mapping experiments. The main purpose is to give an intuitive picture of the possibility and difficulty of the cross correlation.

A. kSZ properties

To understand what role each scale plays in generating kSZ signal, we write Eq.(1) in Fourier space.

The finite box size of 1200 Mpc will only have obvious influence on modes with $k \lesssim 0.005$, we can safely assume the integration on z direction to be from minus infinity to plus infinity. Moreover, the term $a(z)H(z)f(z)$ in Eq.(2) does

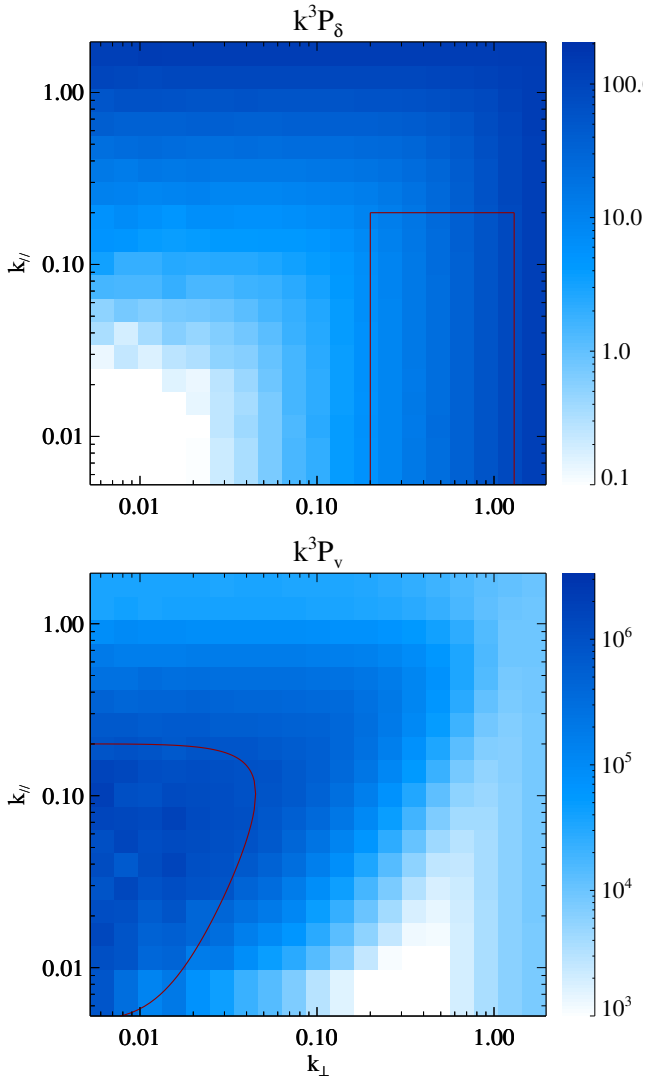

FIG. 1: Illustrating weights of different scales after integration for redshift 1. (Top) The density variance $2\pi^2\Delta^2_\delta \equiv k^3 P_\delta$. (Bottom) The velocity variance $2\pi^2\Delta^2_{v_z} \equiv k^3 P_{v_z}$. Red lines: indicate the most essential modes for generating kSZ signal in ℓ 500 − 3000.

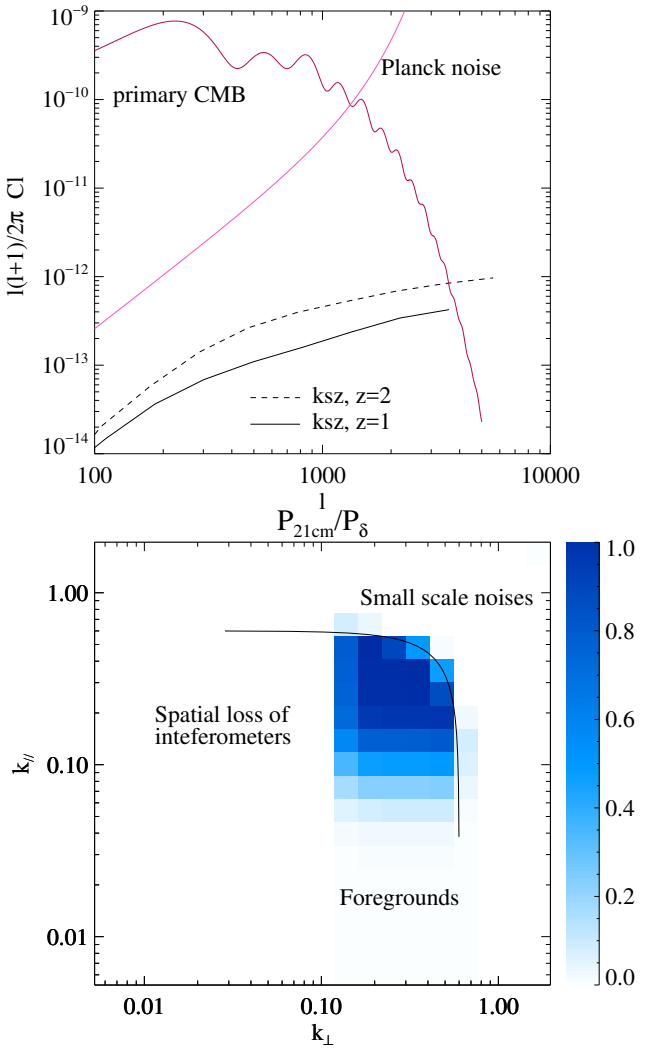

FIG. 2: (Top) Relative strength of angular powerspectrum between primary CMB, Planck noise in 217 GHz band, and kSZ effect in redshift 1 and 2. (Bottom) Demonstrate available modes of density contrasts obtained in realistic 21cm Intensity Mapping experiments. P_{21cm} is the remaining density powerspectrum after noise substraction; P_δ indicates the powerspectrum of a comtact density field.

not vary much in one box, we assume it to be a constant for simplicity. Then the Fourier transformation is just the $k_z = 0$ mode of the momentum $p_\parallel(\boldsymbol{k})$ in Fourier space.

$$\Theta(\boldsymbol{l}) \equiv \ \Theta\ \ (k_x\chi, k_y\chi, 0) \propto \int d^3k'\delta(\boldsymbol{l}/\chi - \boldsymbol{k}'_\perp, k'_\parallel)v_z(\boldsymbol{k'}) \tag{5}$$

An essential feature of Eq.(5) is that in transverse plane, density and velocity field of different scales are multiplied together; while in parallel direction, only δ and v_z with identical k_z are coupled together.

The relative strength of $|\delta(\boldsymbol{k})|$ and $|v_z(\boldsymbol{k})|$ in different scales are implied in Fig.1. It is obvious that the velocity field contributes almost dominantly from large scale structures, leaving little contribution from $k_z > 0.2h/Mpc$ with $k_\perp > 0.02h/Mpc$. This makes it roughly an ellipitical selection functions in the convolution — It selects δ with similar range of k_z and $k_\perp \sim l/\chi - 0.01$ h/Mpc. To see it clearly, let us assume that $|v(\boldsymbol{k})|$ drops fast enough for large k and could be demonstrated as a Delta Function centered at $(k_\perp, k_\parallel) = (0.01, 0.1)$ h/Mpc. then it is immediately shown that

$$\Theta(\boldsymbol{l}) \ \propto \int d^3k'\delta(\boldsymbol{l}/\chi - \boldsymbol{k}'_\perp, k'_\parallel)\delta^D(0.01, 0.1) \tag{6}$$

$$\sim \delta(\boldsymbol{l}/\chi - 0.01, 0.1). \tag{7}$$

Therefore, when generating kSZ signals, it is crucial to have large scale modes for v_z. However, which scale matters most for $\delta(\boldsymbol{k})$ depends on the ℓ we look at.

To decide the targeted ℓ range, there are many factors to consider: the strength of the primary CMB, facility limits

and other fluctuations on CMB such as thermal SZ effect**??** and CMB lensing**??**. Consider using Plank**??** data in the 217 GHz band, where the tSZ signal vanishes, we demonstrate the angular powerspectrum of primary CMB, facility noises, and kSZ of redshift 1 and 2. As shown in Fig.**??**, only in the range of $\ell \sim 500 - 3000$, there is a chance for us to distinguish the kSZ signal.

In Fig.1, we demonstrate the essential modes for mock kSZ signal in both $v_z(\boldsymbol{k})$ and $\delta(\boldsymbol{k})$ fields with red lines. Linearly, velocity field of a certain scale only relates to identical scale of density field, see Eq.(2). Therefore, an ideal cross correlation density field should be comtact in both regions.

Note: all the demonstration figures are towards redshift 1, however there is no distinctive difference for quantitive analysis at redshift 2.

B. 21 cm Intensity Mapping Properties

After understanding the essential modes for kSZ signal, we discuss the current situation ongoing 21cm Intensity Mapping experiments. As mentioned before, the density contrasts obtained from ongoing 21cm intensity mapping experiments maybe degraded by the relatively low resolution, the strong foreground noises and the spatial loss of interferometers. Several simple filters could be used to demonstrate the loss.

1. For small scale noises:

The finite spacial and velocity resolution of facilities prevent us from resolving infinitely small structures in both parallel and perpendicular directions. Therefore we import a cut off scale k_{max} with a Heaviside Function $H(k_{max} - k)$, dropping all the modes with k larger than k_{max}.

2. For foreground noises:

Foregrounds coming from Galactic emissions, telescope noise, extragalactic radio sources and Radio recombination lines, could be three orders brighter than actual signals[12, 13]. The process of foreground removal, taking advantage of its low spectral degrees of freedom [17], will inevitably contaminates the smooth large scale structure in radial direction. To imitate the loss, a high pass filter $W_{fs}(k_\parallel) = 1 - e^{-k_\parallel^2 R_\parallel^2/2}$ is applied to density contraction.

3. For spatial loss of inteferometers:

Large scale structure in perpendicular plane, due to the smoothness, will appear sharp in the visibility function of interferometers after Fourier Transformation. Unfortunately that sharp peak could not be resolved by interferometers due to the incomplete sampling caused by the finite length of the shortest baselines. Therefore, structures with angular sizes greater than a threshold l_{min} are assumed to be lost in our simulations.

In sum, the observed 21 cm density contrasts after all the loss will appear as

$$\delta_{nf}(\boldsymbol{k}) = \delta(\boldsymbol{k}) H(k_{max} - k) W_{fs}(k_\parallel) H(l - l_{min}), \quad (8)$$

The chosen parameters and reasons are presented in Table. I.

The demonstration of a worst case for $z = 1$ is shown in Fig.**??**. As we could see, essential modes for density field are partly resolved. However, the reconstruction of velocity field will be a total failure due to the spatial loss of inteferometers.

If we directly use this density contrast to generate mock kSZ signal, its correlation r (Eq.(**??**)) with real kSZ will be at most 0.2. Luckily, till now we only use the linear theory for reconstruction, while nonlinearly modes of different scales are coupled. If we could identify a relatively clean nonlinear effect in density field, we would be able to retrieve the information needed for velocity reconstruction. The effect we choose is the tidal influence of large scale structure on small scales, following [14, 15].

	z=1		z=2	
[a] $R_\parallel$ Mpc/h	15	60	10	40
[b] k_{max} h/Mpc	0.6	1.2	0.4	0.8
[c] ℓ_{min}	300			

[a]Foreground: smear $k_z \lesssim 0.08, 0.02, 0.12, 0.03$ h/Mpc respectively. Parameters based on [18–20]

[b]Small scale noises: based on CHIME[21] and HIRAX[11] with 100m and 200m longest baseline respectively.

[c]Spatial loss of inteferomenter: assume shortest baseline of 20m.

TABLE I: Parameter of different noise filtering.

IV. ALGORITHM: COSMIC TIDAL RECONSTRUCTION

The evolution of small scale structure is modulated by large scale gravitational force. We can select this effect and solve for the large scale potential.

Consider only the anisotropic influence from tidal force, the distortions on power spectrum can linearly be calculated as

$$\delta P(\boldsymbol{k}, \tau)|_{t_{ij}} \;=\; \hat{k}^i \hat{k}^j t_{ij}^{(0)} P_{1s}(k, \tau) f(k, \tau) \quad (9)$$

where f is the linear coupling function; $P_{1s}(k, \tau)$ is the theoretical small scale linear powerspectrum; and $\delta P(\boldsymbol{k}, \tau)$ is the real distortion from observations.

Hence we can solve for the unknown quantity t_{ij}, which is the tidal force tensor defined as

$$t_{ij} = \Phi_{L,ij} - \nabla^2 \Phi_L \delta_{ij}^D / 3 \quad (10)$$

$\Phi_{L,ij}$ is the second derivative of large scale potential, δ^D is the Dirac function.

With t_{ij}, we calculate the variance of large scale potential Φ_L and get the large scale density contrast $\kappa_{3\mathrm{D}}$.

$$\kappa_{3\mathrm{D}} \sim \nabla^2 \Phi_L = \frac{3}{2} \nabla^{-2} \partial_i \partial_j t_{ij} \quad (11)$$

Since $f(k, \tau)$ increase with k in our interested scales, the distortions are more obvious in small scales. Therefore, the method mainly use the quadratic statistics on small scales to recover the large scale density field. It works best for close linear regions.

Programming steps:

(1) Gaussianize the field, taking $\delta_g = \ln(1 + \delta)$. This is to allieviate the problem that filter W_i in Eq.(14) heavily weights high density regions.

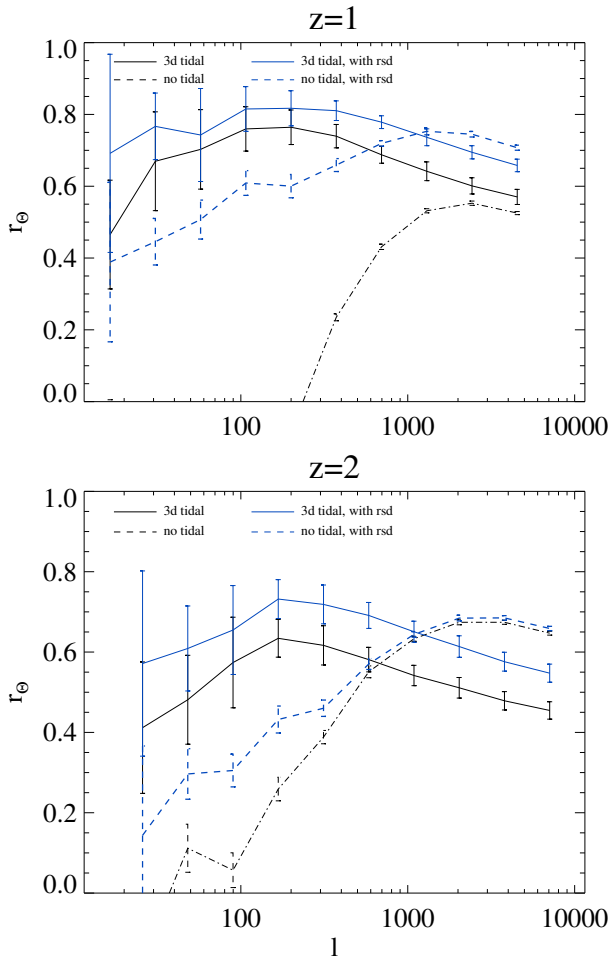

FIG. 3: The cross correlation r between reconstructed kSZ $P_{\hat{\Theta}_{kSZ}}$ and real kSZ $P_{\Theta_{kSZ}}$. (Dashed line) kSZ calculated from foreground filtered 21 cm density field δ_{fs}; (Solid line) kSZ calculated from tidal reconstructed density field. (Blue lines) take into account of redshift space distortions.

(2) Following gravitational lensing procedures, decompose the symmetric, traceless tidal force tensor into 5 components,

$$t_{ij} = \begin{pmatrix} \gamma_1 - \gamma_z & \gamma_\times & \gamma_2 \\ \gamma_\times & -\gamma_1 - \gamma_z & \gamma_y \\ \gamma_2 & \gamma_y & 2\gamma_z \end{pmatrix}. \quad (12)$$

(3) Select density distortions caused by tidal force, by convolving δ_g with a filter W_i deduced from Eq.(9)

$$\delta_g^{w_i}(\boldsymbol{k}) = W_i(\boldsymbol{k})\delta_g(\boldsymbol{k}) \quad (13)$$

$$W_i(\boldsymbol{k}) = i\left[\frac{P(k)f(k)}{P_{tot}^2(k)}\right]^{\frac{1}{2}}\frac{k_i}{k} = S(k)\frac{k_i}{k}$$

where i indicates $\hat{x}, \hat{y}, \hat{z}$ directions, $f(k) = 2\alpha(\tau) - \beta(\tau) d\ln P/d\ln k$ is again the coupling function, with α and β related to linear growth funcion [15], and calculated to be (0.6, 1.3) for $z = 1$ and (0.4, 0.9) for $z = 2$. $P_{tot} = P + P_{noise}$ is observed matter powerspectrum, P is theoretical matter powerspectrum,

(4) Estimate the 5 tidal tensor components from quadratic statistics.

$$\begin{aligned} \hat{\gamma}_1(\boldsymbol{x}) &= [\delta_g^{w_1}(\boldsymbol{x})\delta_g^{w_1}(\boldsymbol{x}) - \delta_g^{w_2}(\boldsymbol{x})\delta_g^{w_2}(\boldsymbol{x})], \\ \hat{\gamma}_2(\boldsymbol{x}) &= [2\delta_g^{w_1}(\boldsymbol{x})\delta_g^{w_2}(\boldsymbol{x})], \\ \hat{\gamma}_x(\boldsymbol{x}) &= [2\delta_g^{w_1}(\boldsymbol{x})\delta_g^{w_3}(\boldsymbol{x})], \\ \hat{\gamma}_y(\boldsymbol{x}) &= [2\delta_g^{w_2}(\boldsymbol{x})\delta_g^{w_3}(\boldsymbol{x})], \\ \hat{\gamma}_z(\boldsymbol{x}) &= \frac{1}{3}[(2\delta_g^{w_3}(\boldsymbol{x})\delta_g^{w_3}(\boldsymbol{x}) \\ &\quad -\delta_g^{w_1}(\boldsymbol{x})\delta_g^{w_1}(\boldsymbol{x}) - \delta_g^{w_2}(\boldsymbol{x})\delta_g^{w_2}(\boldsymbol{x}))], \end{aligned} \quad (14)$$

(5) Reconstruct large scale density contrast κ_{3D} from tidal tensor:

$$\begin{aligned} \kappa_{3D}(\boldsymbol{k}) = \frac{1}{k^2} \quad & [(k_1^2 - k_2^2)\gamma_1(\boldsymbol{k}) + 2k_1k_2\gamma_2(\boldsymbol{k}) \\ & +2k_1k_3\gamma_x(\boldsymbol{k}) + 2k_2k_3\gamma_y(\boldsymbol{k}) \\ & +(2k_3^2 - k_1^2 - k_1^2)\gamma_z(\boldsymbol{k})]. \end{aligned} \quad (15)$$

(6) Correct bias and suppress noise with a Wiener filter.

Due to the foregrounds, the noise in z direction will be different from x,y direction, therefore we apply an anisotropic Wiener filter.

$$\hat{\kappa}_c(\boldsymbol{k}) = \frac{\kappa_{3D}(\boldsymbol{k})}{b(k_\perp, k_\parallel)} W(k_\perp, k_\parallel)\,, \quad (16)$$

Bias $b(k_\perp, k_\parallel) = P_{\mathrm{k3D},\delta}/P_\delta$ is the cross powerspectra between reconstructed field κ3D and original field δ, Wiener filter $W(k_\perp, k_\parallel) = P_\delta/(P_{\mathrm{k3D}}/b^2)$.

Here $\hat{\kappa}_c$ is the output large scale density contrast we obtain from tidal reconstruction. We use it to calculate velocity $\hat{v}_z^{\mathrm{tide}}$.

V. RESULT: CROSS CORRELATION

For comparison, we first present the cross correlation between v_z and $\hat{v}_z^{tide}$ in lower panels of Fig.**??**.

It is obvious that the previously lost small $k_\parallel$ modes are partly recovered. The reconstruction on $k_\parallel$ direction is better than on $k_\perp$ direction. This is because tidal reconstruction relies heavily on large k modes, yet lots of large $k_\perp$ modes, whose $k_\parallel$ is small, are lost in the foregrounds. There is degrading performance of tidal reconstruction on $z = 2$ compared to $z = 1$, which mainly results from the stricter cutoff $k_c = 0.32$ h/Mpc compared to $k_c = 0.5$ h/Mpc.

In Fig.3, we demonstrate the correlation r between the reconstructed kSZ signal $\hat{\Theta}_{tide}$ and original kSZ signal Θ.

It is important to see: For $z = 1$, there are significant improvement on the cross-correlation after tidal reconstruction, especially below $\ell \sim 2000$; for $z = 2$, the cross-correlation is improved for $\ell \lesssim 800$. Combining noise filtered fields and tidal reconstructed fields, we shall have good cross-correlation for $\ell \sim 50 - 5000$, with the assumed level of foregrounds and noises on small scales.

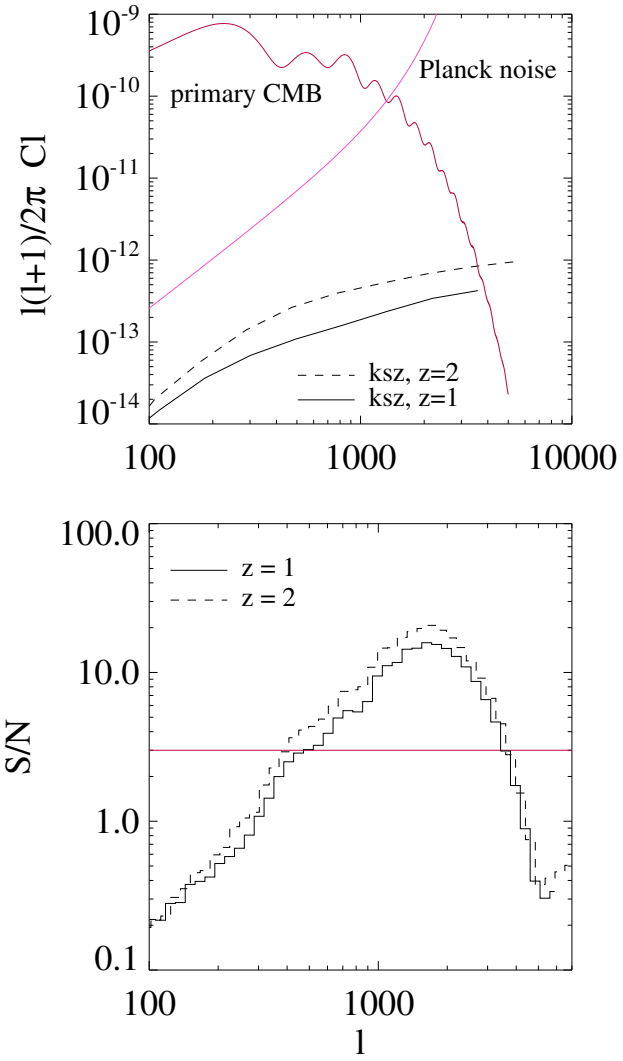

FIG. 4: (Top) Relative strength of kSZ signal, within a box of $\Delta\chi = 1200 Mpc/h$. (Bottom) predicted S/N, assuming Planck noise, $\Delta\ell/\ell = 0.1$, $f_{sky} = 0.8$.

VI. STATISTICAL ERROR AND S/N

We use the statistical error to estimate the S/N ratio for real surveys, taking into account the contamination from primary CMB and facility noises.

$$\frac{S}{N} = \frac{C_l}{\Delta C_l} \simeq r\sqrt{(2\ell+1)\Delta l f_{\rm sky}}\sqrt{\frac{C_l^{\rm kSZ,\Delta z}}{C_l^{\rm CMB}+C_l^{\rm kSZ}+C_l^{\rm CMB,N}}} \quad (17)$$

Where $C_l^{\rm CMB}$ is the angular powerspectrum of primary CMB; $C_l^{\rm CMB,N}$ indicates the facility noises; $C_l^{\rm kSZ,\Delta z}$ is the kSZ signal from a certain redshift bin; r is the correlation coefficients we get; $f_{\rm sky}$ is the percent of sky area covered by both surveys.

In our case, we calculate $C_l^{\rm CMB}$ from CAMB [22]. We use Planck 2015 results [23] at 217GHz to estimate $C_l^{\rm CMB,N}$. $C_l^{\rm CMB,N} = (\sigma_{p,T}\theta_{\rm FWHM})^2 W_l^{-2}$; where $\sigma_{p,T} = 8.7\mu K_{\rm CMB}$ is Sensitivity per beam solid angle, $\theta_{\rm FWHM} \sim 5'$ is the effective beam FWHM, $W_l = \exp[-\ell(\ell+1)/2\ell^2_{\rm beam}]$ is the smoothing window function, with $\ell_{\rm beam} = \sqrt{8\ln 2}/\theta_{\rm FWHM}$. We choose $f_{\rm sky} = 0.8$, since it is feasible for 21 cm intensity mapping to survey large sky areas. We choose $\Delta\ell/\ell = 0.1$. And for $C_l^{\rm kSZ,\Delta z}$, we choose two bins of size 1200 Mpc/h, centered at redshift 1,2 respectively.

In Fig.4, we plot the S/N level for the two redshift bins. The S/N will exceeds 3 from $\ell \sim 500 - 3000$. The overall S/N for $z = 1$ is 45, and for $z = 2$ is 59.

Since we only use the correlation calculated from tidal reconstructed field, the S/N shall be higher for $z = 2$ combining tidal reconstructed field and foreground filtered field.

VII. CONCLUSION

In this paper, we discuss the possibility of cross correlating kSZ signal with 21 cm intensity mapping as a new probe to study baryon distributions. A tomographic way of calculating cross correlation with estimated velocity field is applied. Correlation results are presented for redshift 1 and 2, considering foreground noises, finite telescope resolution, and redshift space distortions. The latter two will not matter much. However, the foreground noise will smear the correlation on large scales while leaving sufficient correlation on smaller scales such as $\ell \sim 1000$. In order to study the large scale baryon distribution, we recover modes lost in foregrounds with a 3D tidal reconstruction and obtain a $r > 0.6$ correlation for $\ell \sim 100 - 2000$. After the reconstruction, we will likely be able to distinguish cross correlation signals from $\ell \gtrsim 500$. Assuming Planch noise, the total S/N can reach 45 for $z = 1$ and 59 for $z = 2$. This shows a promising future for this method.

VIII. ACKNOWLEDGE

We acknowledge discussions with Kendrick Smith, Matthew Johnson, Wenkai Hu, Tianxiang Mao and Jiawei Shao. The simulations were performed on the BGQ supercomputer at the SciNet HPC Consortium. SciNet is funded by: the Canada Foundation for Innovation under the auspices of Compute Canada; the Government of Ontario; the Ontario Research Fund – Research Excellence; and the University of Toronto. Research at the Perimeter Institute is supported by the Government of Canada through Industry Canada and by the Province of Ontario through the Ministry of Research & Innovation. The Dunlap Institute is funded through an endowment established by the David Dunlap family and the University of Toronto.

[1] U.-L. Pen, ApJ **510**, L1 (1999), astro-ph/9811045.

[2] A. M. Sołtan, A&A **460**, 59 (2006), astro-ph/0604465.

[3] R. A. Sunyaev and Y. B. Zeldovich, Comments on Astrophysics and Space Physics **4**, 173 (1972).

[4] R. A. Sunyaev and I. B. Zeldovich, MNRAS **190**, 413 (1980).

[5] E. T. Vishniac, ApJ **322**, 597 (1987).

[6] M. Fukugita and P. J. E. Peebles, ApJ **616**, 643 (2004), astro-ph/0406095.

[7] N. Hand, G. E. Addison, E. Aubourg, N. Battaglia, E. S. Battistelli, D. Bizyaev, J. R. Bond, H. Brewington, J. Brinkmann, B. R. Brown, et al., Physical Review Letters **109**, 041101 (2012), 1203.4219.

[8] J. Shao, P. Zhang, W. Lin, Y. Jing, and J. Pan, MNRAS **413**, 628 (2011), 1004.1301.

[9] M. Li, R. E. Angulo, S. D. M. White, and J. Jasche, MNRAS **443**, 2311 (2014), 1404.0007.

[10] Y. Xu, X. Wang, and X. Chen, ApJ **798**, 40 (2015), 1410.7794.

[11] http://www.acru.ukzn.ac.za/ hirax/.

[12] T. Di Matteo, B. Ciardi, and F. Miniati, MNRAS **355**, 1053 (2004), astro-ph/0402322.

[13] K. W. Masui, E. R. Switzer, N. Banavar, K. Bandura, C. Blake, L.-M. Calin, T.-C. Chang, X. Chen, Y.-C. Li, Y.-W. Liao, et al., ApJ **763**, L20 (2013), 1208.0331.

[14] U.-L. Pen, R. Sheth, J. Harnois-Deraps, X. Chen, and Z. Li, ArXiv e-prints (2012), 1202.5804.

[15] H.-M. Zhu, U.-L. Pen, Y. Yu, X. Er, and X. Chen, ArXiv e-prints (2015), 1511.04680.

[16] J. Harnois-Déraps, U.-L. Pen, I. T. Iliev, H. Merz, J. D. Emberson, and V. Desjacques, MNRAS **436**, 540 (2013), 1208.5098.

[17] E. R. Switzer, T.-C. Chang, K. W. Masui, U.-L. Pen, and T. C. Voytek, ApJ **815**, 51 (2015), 1504.07527.

[18] K. W. Masui, E. R. Switzer, N. Banavar, K. Bandura, C. Blake, L.-M. Calin, T.-C. Chang, X. Chen, Y.-C. Li, Y.-W. Liao, et al., ApJ **763**, L20 (2013), 1208.0331.

[19] E. R. Switzer, K. W. Masui, K. Bandura, L.-M. Calin, T.-C. Chang, X.-L. Chen, Y.-C. Li, Y.-W. Liao, A. Natarajan, U.-L. Pen, et al., MNRAS **434**, L46 (2013), 1304.3712.

[20] J. R. Shaw, K. Sigurdson, M. Sitwell, A. Stebbins, and U.-L. Pen, Phys. Rev. D **91**, 083514 (2015), 1401.2095.

[21] K. Bandura, G. E. Addison, M. Amiri, J. R. Bond, D. Campbell-Wilson, L. Connor, J.-F. Cliche, G. Davis, M. Deng, N. Denman, et al., in *Society of Photo-Optical Instrumentation Engineers (SPIE) Conference Series* (2014), vol. 9145 of *Society of Photo-Optical Instrumentation Engineers (SPIE) Conference Series*, p. 22, 1406.2288.

[22] A. Lewis, A. Challinor, and A. Lasenby, Astrophys. J. **538**, 473 (2000), astro-ph/9911177.

[23] Planck Collaboration, R. Adam, P. A. R. Ade, N. Aghanim, M. Arnaud, M. Ashdown, J. Aumont, C. Baccigalupi, A. J. Banday, R. B. Barreiro, et al., ArXiv e-prints (2015), 1502.01587.